Themistocles L. Resvanis[2]
Mem. ASME
Department of Mechanical Engineering,
Massachusetts Institute of Technology,
Cambridge, MA 02139
e-mail: resvanis@mit.edu

Zhibiao Rao
Department of Mechanical Engineering,
Massachusetts Institute of Technology,
Cambridge, MA 02139
e-mail: zbrao@mit.edu

J. Kim Vandiver
Professor of Mechanical and Ocean Engineering,
Mem. ASME
Department of Mechanical Engineering,
Massachusetts Institute of Technology,
Cambridge, MA 02139
e-mail: kimv@mit.edu

Effects of Strake Coverage and Marine Growth on Flexible Cylinder Vortex-Induced Vibrations[1]

This paper presents some results from the recent SHELL tests at the MARINTEK basin. The tests involved towing densely instrumented flexible cylinders at Reynolds numbers up to 220,000. The main objective is to present the experimental results describing the effectiveness of different amounts of strake coverage and to explore the influence of simulated marine growth. The data are presented in terms of cross-flow (CF) response amplitudes and rainflow-counted damage rates due to the combined CF and in-line (IL) bending stresses. All the results are compared with the bare cylinder cases which will be used as a reference to determine how effective the strakes are in suppressing vortex-induced vibrations (VIV) and how this effectiveness can be affected by marine growth. The results show that even small bare sections (missing strakes) can lead to significant VIV response. Finally, the tests revealed that even moderate amounts of marine growth can quickly negate any suppression coming from the strakes. [DOI: 10.1115/1.4033821]

1 Introduction

As oil and gas exploration and production moves into deeper and deeper waters, the fatigue damage accumulated due to VIV is quickly becoming one of the most critical aspects of deep-water riser design. The helical strakes and other suppression devices are commonly used to try and minimize the effects of VIV. They work by ensuring that the flow separation points are not aligned along the structure or by moving the reattachment points further downstream of the cylinder. In any case, they interrupt the coherence of the shed vortex sheet, thus minimizing the power into the structure.

Several strake and fairing designs have been shown to be extremely effective in disrupting VIV on fully covered flexible cylinders. The question that remains to be answered is how much strake coverage is actually necessary to minimize VIV on a flexible cylinder or conversely how many strakes can one lose before VIV becomes a serious source of fatigue damage on the now partially straked riser.

The other pressing issue that needs to be addressed once a strake design and coverage has been chosen is to determine how the suppression characteristics of the chosen device will be affected by the inevitable presence of the marine growth. This might be done in order to determine a cleaning schedule or to simply account for the accumulated damage so that one has more confidence in the design or future operation of the riser.

This work makes use of test data gathered on behalf of SHELL International Exploration and Production Co., by MARINTEK. The tests involved towing three different 38-m long flexible pipes/cylinders in uniform and sheared currents with different suppression devices, amounts of strake coverage, and simulated marine growth.

The first part of this paper proposes a framework for experimentally determining the worst possible combination of CF and IL damage, i.e., the method identifies the position around the circumference of the cylinder's cross section that will experience the most severe loading due to the simultaneous motion in both CF and IL directions. In the vast majority of cases analyzed, the most damaging combination of IL and CF motion results in a damage rate very similar in magnitude to the pure CF signals, and the position or orientation around the circumference of the cross section where this occurs is usually very close to or coincides with the CF direction.

The second part of this paper focuses on how effectively four different strake coverage amounts suppress VIV. The data are presented in terms of response amplitudes and damage rates, and it is demonstrated that the large reduction in damage rate when strakes are used is primarily due to the elimination of higher harmonics rather than simply being the result of smaller response amplitudes.

Finally, the tests analyzing the effects of simulated marine growth demonstrate that even small amounts of marine growth can quickly alter the efficiency of a specific strake design and lead to damage rates that are many times higher than those expected with clean strakes.

2 Description of Experiments

The 38 m SHELL experiments were conducted at MARINTEK's ocean basin on behalf of SHELL International Exploration and Production Co. The experiment involved testing three densely instrumented cylinders of different diameters. The flexible cylinders were mounted under a carriage that could traverse the basin in a manner capable of simulating both uniform and linearly sheared flows. The full test matrix included runs which tested the effects of fairings, strakes, staggered buoyancy, and marine growth on riser response. A most interesting feature of this data set was the very large range of Reynolds numbers covered while testing the three different pipes. The towing velocities ranged from 0.25 m/s to 3.45 m/s which correspond to a Reynolds number range from 5000 to 220,000. More details on the experimental setup can be found in Refs. [1] and [2].

This work primarily focuses on analyzing the data obtained for the response of the largest diameter model, pipe 3. The cylinder properties are listed in Table 1. Table 2 summarizes all the test cases used in the analysis presented in this paper. The table lists

[1]An abridged version of this paper was originally presented at the 33rd International Conference on Ocean, Offshore and Arctic Engineering and subsequently published in the conference proceedings as OMAE2014-24462.

[2]Corresponding author.

Contributed by the Ocean, Offshore, and Arctic Engineering Division of ASME for publication in the JOURNAL OF OFFSHORE MECHANICS AND ARCTIC ENGINEERING. Manuscript received July 29, 2015; final manuscript received May 27, 2016; published online June 27, 2016. Assoc. Editor: Celso P. Pesce.

Table 1 Flexible cylinder properties

Length (m)	38
Outer diam. or hydrodynamic diam. (mm)	80
Optical diam. or strength diam. (mm)	27
Inner diameter (mm)	21
EI ($N{\cdot}m^2$)	572.3
E (N/m^2)	3.46×10^{10}
Mass in air with contents (kg/m)	5.708
Mass in water with contents (kg/m)	0.937
Mass ratio	1.14

the strake coverage/configuration, whether marine growth was applied, and the range of towing velocities tested in both uniform and sheared flows for each configuration. The dominant excited modes for the 80 mm diameter, bare cylinder tests in uniform flows, ranged between modes 2 and 7 for towing speeds between 0.5 m/s and 1.8 m/s, respectively.

The pipe had fiber optic, Bragg strain gauges at 30 different locations and accelerometers at 22 locations along the span in both the CF and IL directions. The curvature/strain was measured at a distance of 13.5 mm from the neutral axis and all sensors were sampled at a rate of 1200 Hz. Damping tests, conducted in air, yielded structural damping ratios of $\sim 0.5 - 0.7\%$ of critical.

The triple start helical strakes were made from polyurethane and were delivered in sections 0.43 m long. Each section was made of two halves which were 'clamped' around the cylinder and held together with zip ties. The half-sections had thicknesses of 3 mm, thus increasing the cylinder's outer diameter to 86 mm. The strake design called for a fin height equal to 25% of the outer diameter and a pitch equal to 15 diameters.

A small gap was left between every five buoyancy modules such that the coverage would be similar to the best that could be done on a typical marine riser with connectors. This resulted in an $\sim$83% effective coverage. This will be referred to as the fully covered case.

After testing the cylinder while it was fully covered with strakes, the test matrix called for removing sections of the strakes from the midspan in order to create continuous bare gaps equal to 5%, 15%, 25%, and 50% of the model's length. Figure 1 is a photograph showing the strake design and a small bare section.

The marine growth was only applied on the fully straked cylinder ($\sim$83% coverage). The carpeting used to simulate the soft marine growth had two different heights corresponding to 30% and 60% of the fin height. It is important to note that the marine growth was only applied around the circumference of the cylinder and not on the fins themselves, as shown in Fig. 2. Applying the simulated marine growth in this manner was more practical than trying to cover the fins. Furthermore, it was an attempt to model the worst possible effects of the marine growth since it is well known that the suppression capabilities of strakes depend strongly on the ratio of the fin height to cylinder diameter.

Table 2 Test matrix of cases used in present analysis

Strake configuration	Marine growth	Uniform-flow speeds (m/s)	Sheared-flow speeds (m/s)
Bare	None	0.5–1.8	0.5–3.0
50% gap	None	0.25–1.5	N.A.
25% gap	None	0.25–1.5	N.A.
15% gap	None	0.25–1.5	N.A.
5% gap	None	0.25–1.5	N.A.
Full coverage	None	0.25–1.5	N.A.
Full coverage	30% high	0.25–1.5	0.25–1.5
Full coverage	60% high	0.25–1.5	0.25–1.5
Full coverage	30% high only between $0 < x/L < 0.4$	0.25–1.5	0.25–1.5

Fig. 1 Photograph of straked and bare sections

The interested reader is referred to the experiments by Baarholm and Skaugset [3,4] which very carefully investigated the effects of marine growth on straked rigid cylinders and analyzed different methods for simulating the marine growth on strakes. Their work is one of the most systematic attempts to simulate the marine growth on strakes. Their results are not directly comparable to the data analyzed in this paper because this work deals with flexible cylinders and because of the differences in the application of the simulated growth on the strake surfaces.

3 Data Analysis

Many of the data processing techniques used in this work are standard in the VIV model-testing community, details can be found in Refs. [5] and [6]. The data analysis procedures are discussed here to the extent necessary for a reader to understand where the data presented in the following sections originated.

The amplitude at every accelerometer location was determined by double-integrating the accelerometer time-histories in the frequency domain. To account for the possibility that the location where the maximum response occurred between the two measurement locations, a modal reconstruction was performed using both the available curvature response data and the amplitude data.

Response spectra were typically obtained by averaging the information from several neighboring curvature sensors. All time series were high-pass filtered with a cutoff of 0.7 Hz in order to remove any mean components that are not particularly relevant to VIV analysis. Unless otherwise noted, all higher harmonics were taken into account in the analysis and their effects are included in the plotted data.

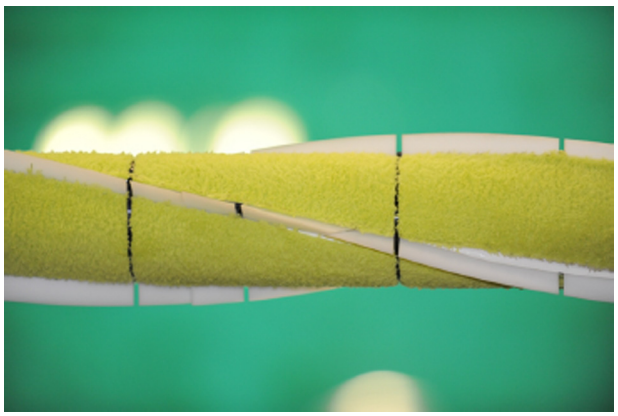

Fig. 2 Photograph of strakes with simulated marine growth

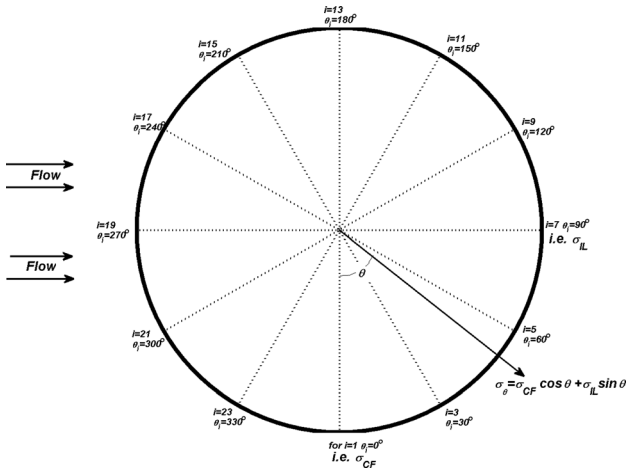

Fig. 3 Cylinder cross section showing the combination of σ_{CF} and σ_{IL} at some arbitrary angle θ_I

3.1 Need for Rainflow-Counting. It is conceivable that due to the complicated motion of the cylinder while undergoing VIV, the most damaging location around the circumference of the cross section does not coincide with the CF or IL directions but rather at some angle between the two.

The stresses and damage rates were computed at 24 orientations ($I = 1,2,\ldots,24$) around the circumference of the cross section as shown in Fig. 3. This was done at every sensor location along the pipe length.

At each circumferential position, the stress time-history, $\boldsymbol{\sigma}_{\theta_i}$, was computed by the vector addition of the CF and IL stress signals, $\boldsymbol{\sigma}_{CF}$ and $\boldsymbol{\sigma}_{IL}$, respectively, as shown in the equation given below

$$\boldsymbol{\sigma}_{\theta_i}(t) = \boldsymbol{\sigma}_{CF}(t)\cos\theta_i + \boldsymbol{\sigma}_{IL}(t)\sin\theta_i \tag{1}$$

Figure 4 shows the results of this vector addition and the resulting stress time-histories at the angles corresponding to $\theta = 0$ deg (i.e., CF direction), $\theta = 30$ deg, $\theta = 60$ deg, and $\theta = 90$ deg (i.e., IL direction). At every angle, θ_i, each stress time-history is rain-flow counted. The most damaging orientation is chosen and labeled as the 'combined stress' or 'combined damage' for each one of the 30 locations along the length of the cylinder where the CF and IL strain gauges are located.

The main motivation for combining the stress components as a function of orientation is to correctly account for the various frequency components in the damage rate estimates. The idea is based on the analysis presented in Ref. [7], the main difference being that in this work rain-flow counting was used whereas the authors in Ref. [5] calculated a damage index based on the root-mean-square (RMS) stresses for both the CF and IL directions and their respective response frequencies and only then applied the coordinate transformation similar to Eq. (1) to their RMS quantities.

Estimating the fatigue life (or damage rate) for a perfectly sinusoidal stress time-history is a straightforward procedure. Similarly, if the stress time-history is narrow-band Gaussian, once again the analytic expressions for damage rate can be derived as shown in Ref. [8]. If the signal contains multiple frequencies and the response amplitude varies significantly, one has no other choice except to revert to cycle counting. Cycle counting algorithms apply Miner's law by examining every half-oscillation in a time-history and sorting the results into bins depending on the amplitude of the examined half-cycle.

From Fig. 4, it should be apparent that after applying the coordinate transformation given by Eq. (1), the stress time-histories contain multiple frequencies and a lot of variability in the amplitude. In this paper, the rain-flow counting algorithm as found in the WAFO toolbox [9] is used to estimate the actual damage accumulated by the cylinder during each test.

Since fatigue properties are not available for the exact composite material that the flexible cylinder was made of, all fatigue calculations assume that it was made of steel with an S–N curve defined according to the DNV-F curve (i.e., $\log(a) = 11.378$ and $m = 3.0$ [10]).

Figure 5 shows the response of the fully bare pipe under a uniform flow excitation of 1.4 m/s. The top plot shows the CF and IL displacements as calculated by the modal reconstructions.

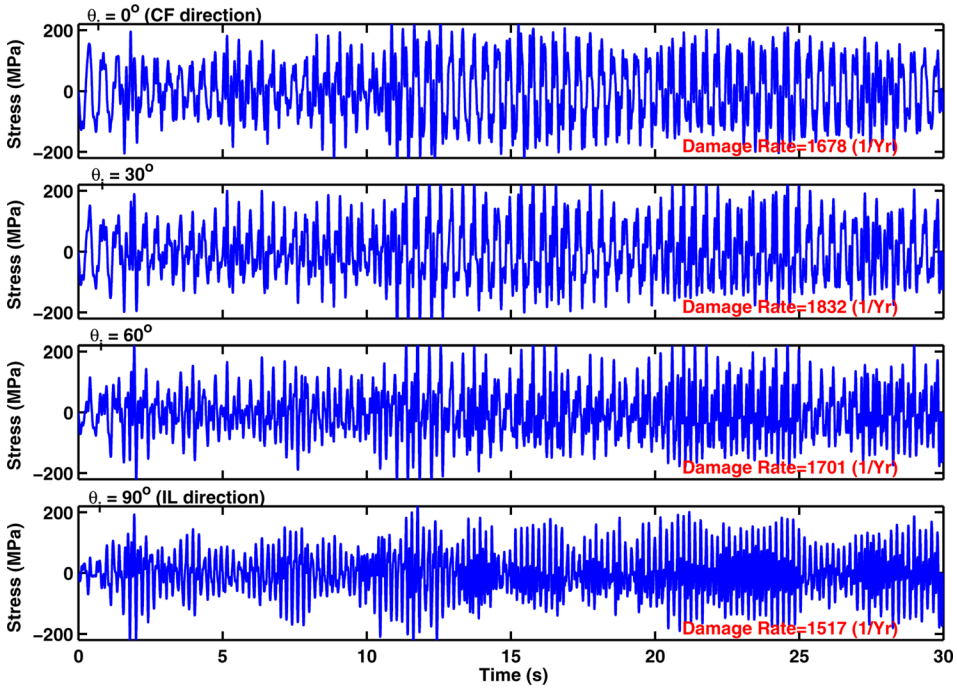

Fig. 4 The stress time-histories at four different four different locations around the circumference of the cross section: $\theta = 0$ (i.e., CF), $\theta = 30$ deg, $\theta = 60$ deg, and $\theta = 90$ deg (i.e., IL) around the circumference of the cross section at a position $x/L \sim 0.06$ along the cylinder length

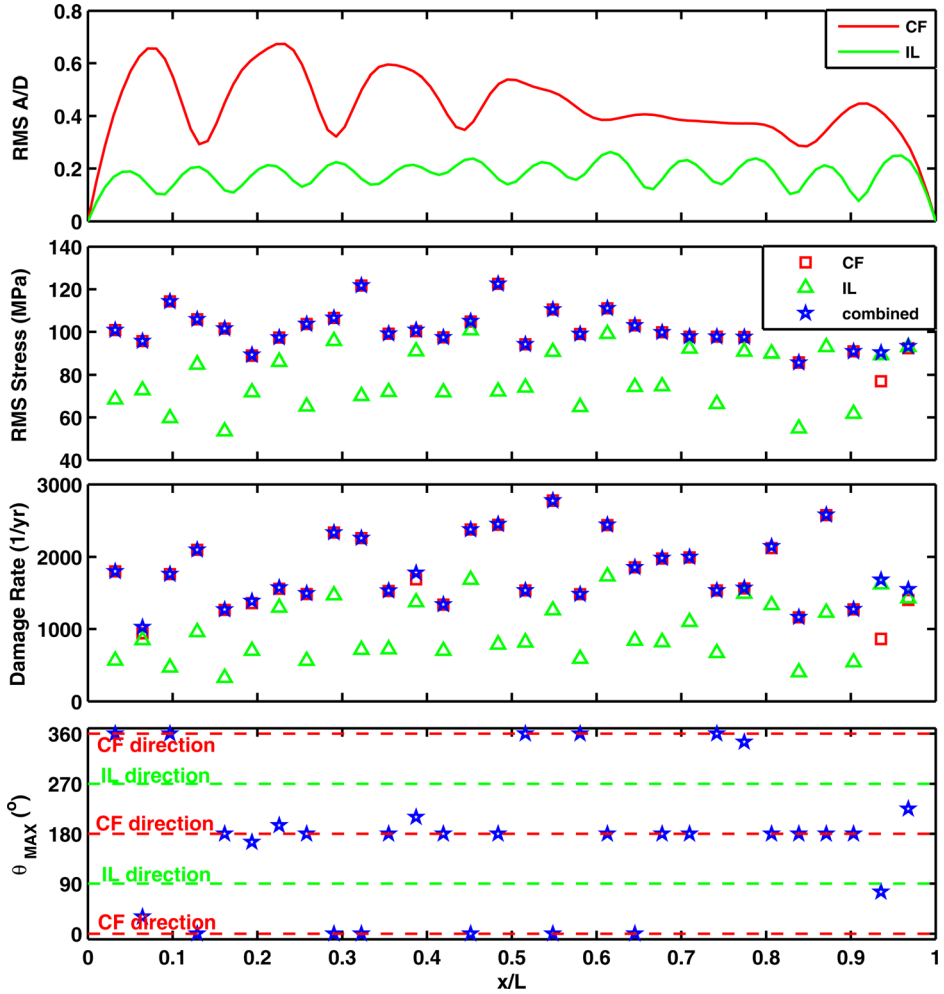

Fig. 5 VIV Response under uniform flow conditions of 1.4 m/s (test 4010) for the bare cylinder. Top: CF and IL RMS response amplitude; second from top: CF and IL RMS stresses (MPa) and the largest combination of the signals in both directions; third from top: CF and IL damage rates (1/yr) and the most damaging combination of the signals in both directions; and bottom: angle around the circumference of the cross section where the most damaging combination of CF and IL damage occurs.

Observe that even though the IL response amplitude is much smaller, there are certain locations where the IL stresses are of comparable magnitude to the CF stresses! This happens because even though the IL response amplitude is significantly smaller than the CF amplitude, the IL wavenumber is much greater than the CF wavenumber due to the approximately two times higher response frequency. The relationship between stresses and amplitude for a flexural wave on a beam is shown in Eq. (2). Here, σ is a stress, E is the Young's Modulus, ε is the bending related strain, A is the response amplitude at a specific time instant, $OD/2$ is the distance from the neutral axis at which the stresses/strains were measured (13.5 mm), and k is the wavenumber

$$\sigma = E\varepsilon = \mathrm{EA}\frac{OD}{2}k^2 \tag{2}$$

Figure 5 also shows the damage rate along the span of the cylinder. Each location has two data points corresponding to the damage rates as calculated from the CF and IL stress time-histories and a third data point corresponding to the damage rate from the most damaging combination of the CF and IL stress time-histories according to Eq. (1). The last plot shows the angle around the circumference of the cross section at which the most damaging combination of CF and IL occurred. Note that even though the combined damage rate at most sensor locations tends to coincide with the CF direction, there are a few locations where this is not the case.

4 Results and Discussion

4.1 Bare Pipes. Figure 6(*a*) shows the maximum damage rate along the pipe span as a function of towing speed for the uniform flow tests. For each test/flow speed, there are three values: the damage rates for the CF and IL directions as well as the most damaging combination of the two around the circumference of the cylinder. Similarly, Fig. 6(*b*) shows the maximum damage rates for the sheared flow tests. For both uniform and sheared flow tests, the IL rate is typically smaller than the CF but still of the same order of magnitude. Note that the worst possible combination of the two coincides or is virtually identical to the CF damage calculation suggesting that the most damaging position around the circumference tends to be at or very close to the CF direction. This is also demonstrated for a specific test in the last plot of Fig. 5.

The stress signals used for plotting Figs. 6(*a*) and 6(*b*) contained large amounts of higher harmonics (3X and 5X for the CF and 4X for the IL directions) as is typically observed in high mode number model testing. Figures 7(*a*) and 7(*b*) show what would happen if the CF and IL signals had been band-pass filtered

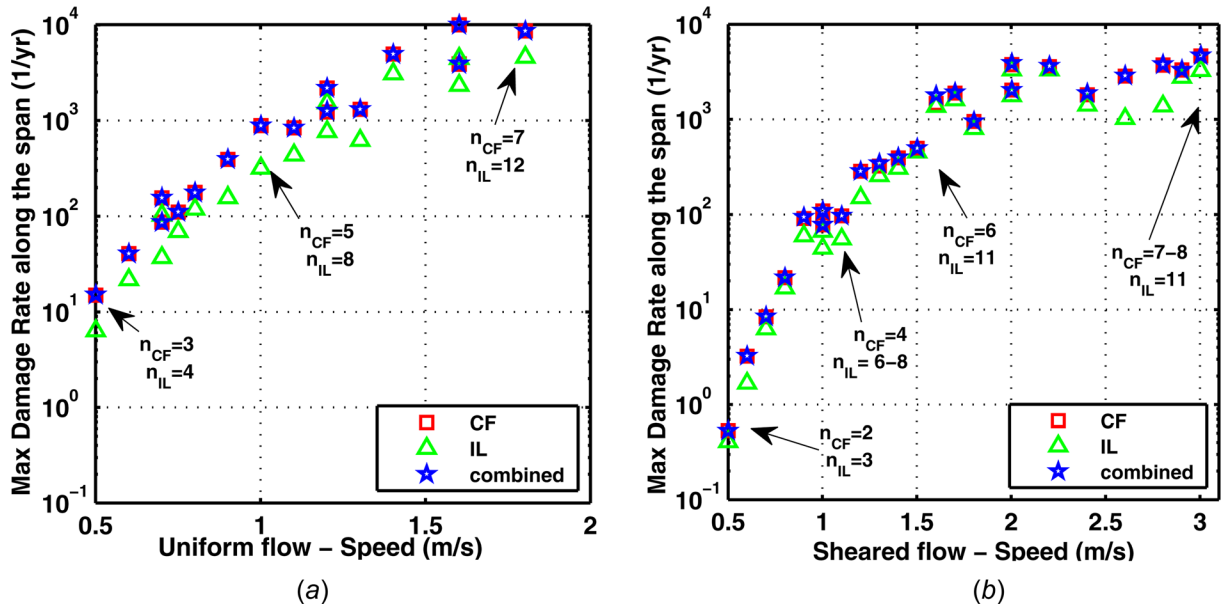

Fig. 6 Maximum damage rate (1/yr) versus towing speed (m/s) in (*a*) uniform flows and (*b*) sheared flows. Data shown includes all higher harmonics. CF and IL excited modes listed for a few selected cases.

around the 1X and 2X frequencies, respectively. Very similar trends are observed with the exception that now there are a few cases where the worst possible damage calculation around the cross section coincides with the IL signal/direction. This happens because the CF signal no longer includes the 3X and 5X components which greatly affect the damage rate due to their high frequencies.

In any case, the worst possible damage rate around the circumference of the cross section (i.e., the 'combined damage') and the IL damage rate are always of the same order of magnitude as the CF damage rate. Resvanis [11] repeats the same analysis for the medium-sized cylinder (30 mm) which typically responded at higher mode numbers and shows that the trends and observations are virtually identical to the information presented in this paper, which focuses exclusively on the largest size cylinder (80 mm). Finally, even though Tognarelli et al. [7] used a slightly different methodology to compute the most damaging combination of IL and CF damage rates, the results they presented agree with the trends identified in Figs. 6(*a*) and 6(*b*), namely that the worst possible damage rate around the cylinder's cross section due to the simultaneous motion in the CF and IL directions coincides with the CF damage rate in the vast majority of cases analyzed.

The aim of this section was not to dismiss the importance of IL motion; on the contrary, the intention was to carefully measure the fatigue caused by the IL motion and demonstrate experimentally that the worst possible damage accumulated anywhere around the cross section is very close to the CF damage rate. If one can conservatively design for CF VIV, then one should be confident that they have accounted for the worst possible case of combined CF and IL VIV.

4.2 Strake Coverage. Figure 8 shows the response for a partially straked cylinder with a bare gap 15% of the total length

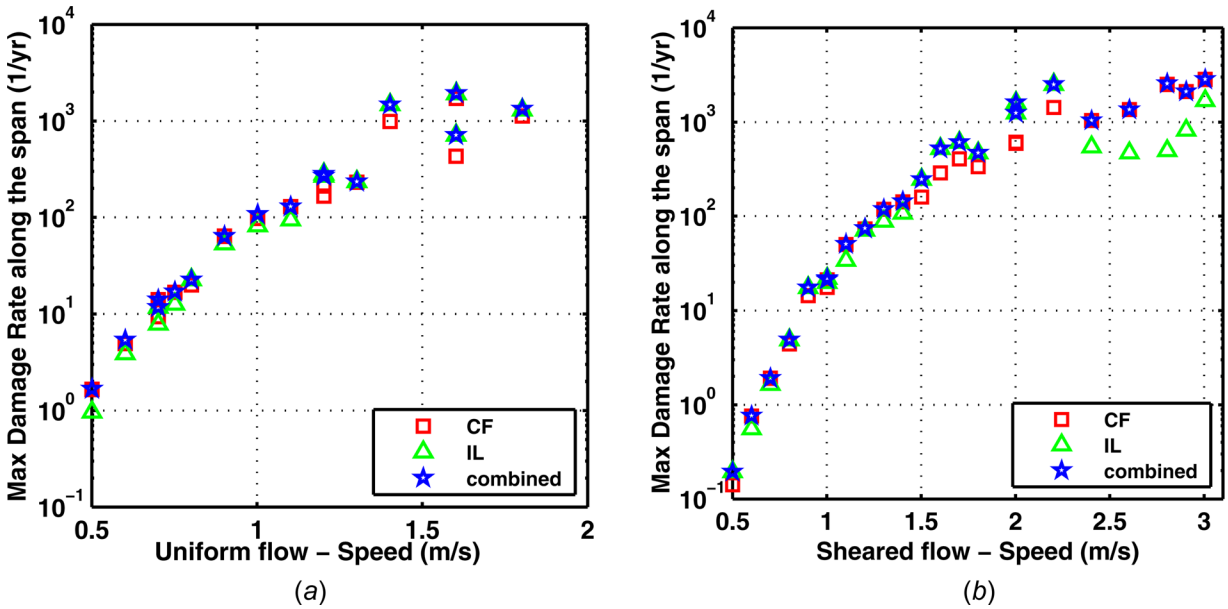

Fig. 7 Maximum damage rate (1/yr) versus towing speed (m/s) in (*a*) uniform flows and (*b*) sheared flows. Data shown excludes all higher harmonics.

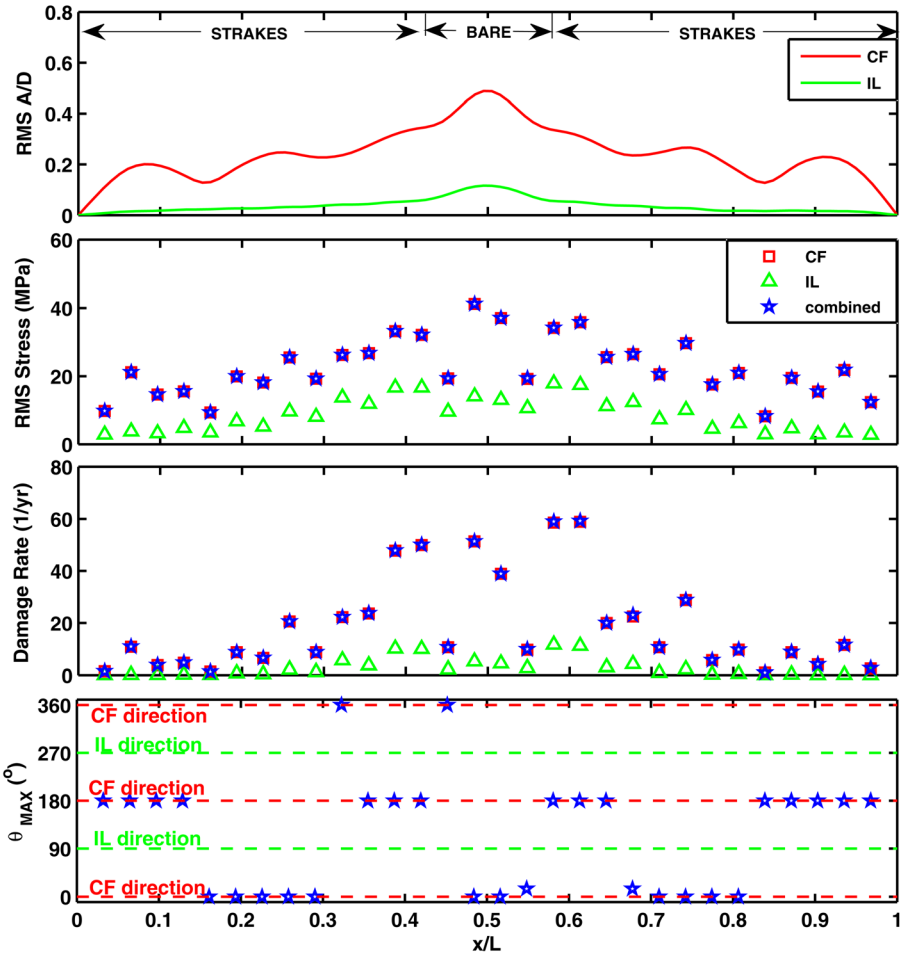

Fig. 8 VIV Response under uniform flow conditions of 1.5 m/s (test 5021) for the straked cylinder with a 15% long gap in the middle. Top: CF and IL RMS response amplitude; second from top: CF and IL RMS stresses (MPa) and the largest combination of the signals in both directions; third from top: CF and IL damage rates (1/yr) and the most damaging combination of the signals in both directions; and bottom: angle around the circumference of the cross section where the most damaging combination of CF and IL damage occurs.

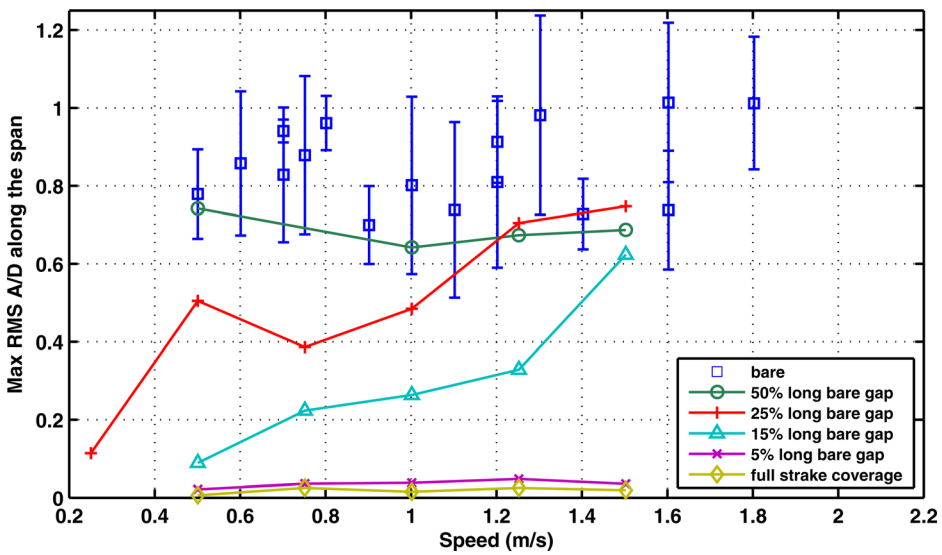

Fig. 9 Maximum RMS CF Amplitude at any location along the span versus towing speed (m/s) in uniform flows. The 'error bars' indicate the temporal variability of the RMS response computed using a short duration moving window over the entire record length.

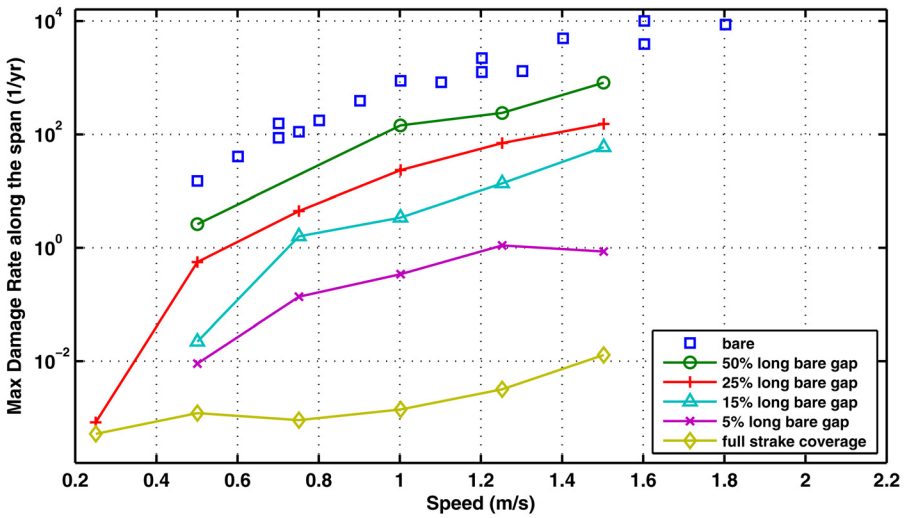

Fig. 10 Maximum damage rate (1/yr) at any location along the span versus towing speed (m/s) in uniform flows

located in the middle. As expected, the largest response amplitude is located in the middle and the response decays as one moves toward either boundary due to the large amounts of hydrodynamic damping introduced by the strakes. Note that because the damage rates have been rainflow-counted and not calculated using analytic expressions, the spanwise location where the largest damage rate occurs does not have to coincide with the location where the largest stress is observed. For most of the partially straked cases that had nonzero response amplitudes, the most damaging location along the riser was located either within the bare regions or immediately adjacent to the straked/bare interface, but within the straked region.

As discussed earlier, four different partial strake coverages were tested in this set of experiments. Figure 9 compares the effectiveness of these different coverage amounts in suppressing VIV by comparing the CF response amplitude with that of the fully bare cylinder as a function of towing velocity (or current speed). A small portion of the scatter in the bare cylinder response data can be attributed to reduced velocity effects but it is primarily due to the stochastic nature of VIV. This is illustrated through the use of 'error bars' which serve to indicate the range of observed values that the RMS amplitude could take depending on the portion of the time signal used for analysis. Details on calculating and using such 'error bars' to represent the variability that exists in VIV response data can be found in Ref. [11].

Figure 10 compares the maximum damage rate along the cylinder with that recorded for the bare cylinder. The damage rate reported is that due to the worst possible combination of CF and IL motion according to methodology described earlier, however, this tends to coincide with the CF direction due to the very small IL motion that results after adding the strakes.

Observe, that the reduction in damage rate is much more dramatic than the reduction of amplitude for a given strake coverage. The reasons for this become obvious after examining a typical response spectrum for the partial strake coverage tests. Figure 11 shows the averaged power spectral density (PSD) of all CF strain gauges along the length of the pipe when the flow speed was 1 m/s. Four different lines are plotted for the bare, 50% and 25% long bare gaps in the middle as well as the fully straked cases. Note that the 3X and 5X peaks for the partial strake coverage cases are greatly reduced when compared to the bare cylinder case. In fact, the fully straked case manages to suppress the higher harmonics entirely.

The resulting reduction in amplitudes and damage rates is due to the following reasons:

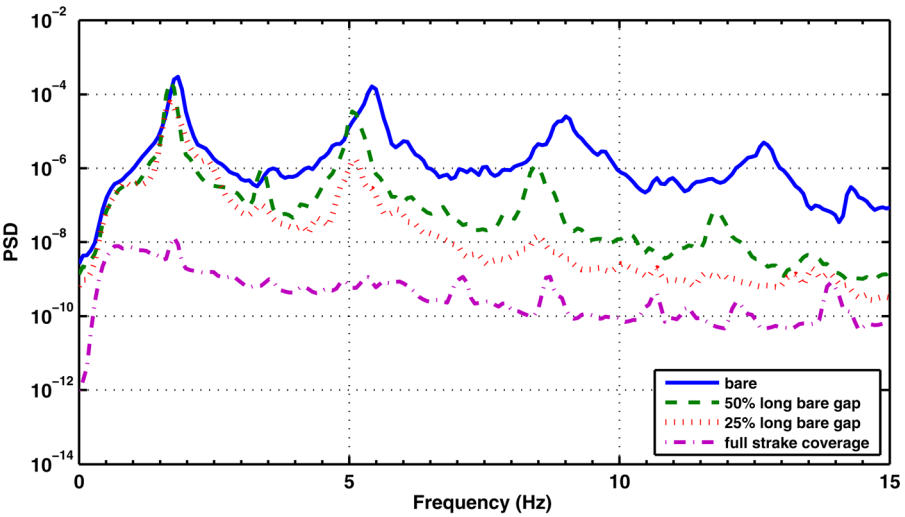

Fig. 11 Averaged PSD from all CF sensors for uniform flow of 1 m/s, effects of strake coverage

- The presence of straked sections will tend to restrict the 'power-in' regions to the bare sections only. This has the effect of reducing the length of the cylinder available for power input to the structure and simultaneously increasing the power out of the structure by allowing a portion of the structure to contribute to the hydrodynamic damping [12].
- Straked sections that belong to the power-out regions will contribute more to the hydrodynamic damping than a bare section of similar length [13].

The above reasons, are really only applicable to strake configurations with sizeable bare sections. For the fully straked cases and the cases with 5% long bare sections in the middle, examination of the spectra revealed that the excitation is being driven entirely by the straked sections. In these situations, the VIV amplitude and damage rates are very small because of the very small lift coefficients and the lack of span-wise coherence of the wake. As mentioned previously, the very small damage rates measured are due to a combination of very small response amplitudes and negligible higher harmonics.

4.3 Strake Efficiency. Strake efficiency is a commonly used concept which is rarely explicitly defined. Here the strake or suppression efficiency is defined as the ratio between the CF VIV response amplitude reduction with strakes to the response amplitude of the bare cylinder (see Eq. (3)). The measurements are most often made on a spring-mounted rigid cylinder in a towing tank. The cylinder is either 100% bare or 100% covered by strakes during testing. The damping of the spring-mounted cylinder is usually very small or forced to be zero by means of a feedback controlled negative damping force (i.e., a force to null-out the effects of the real mechanical damping present in the system)

$$\text{suppression efficiency} = \frac{A/D_{\text{bare}} - A/D_{\text{straked}}}{A/D_{\text{bare}}} \tag{3}$$

Extending the concept of strake efficiency to flexible cylinders is risky and likely to lead to very inappropriate use of strakes in real conditions. Even if one tried to compute some spatial averages of the response amplitude on the flexible cylinder, he would still have to choose specific regions of the riser to compute these spatial averages and as shown in Fig. 8, the response amplitude for a partially straked riser varies greatly between the straked and bare regions.

There is only one circumstance in which the concept has a similar interpretation to that of a spring-mounted rigid cylinder. That is the case of a fully straked flexible cylinder in a uniform flow. In this case, one could define the efficiency as the ratio of CF response amplitude reduction with strakes to that without strakes under peak response, resonant lock-in conditions. Only for such simple cases, it is possible to predict the approximate behavior of a riser with strakes by using the measured performance from towing tank qualification tests on rigid cylinders. Even in this idealized case, defining a strake 'efficiency' simply in terms of response amplitude overlooks the fact that strakes suppress higher harmonics, thus greatly extending fatigue life by eliminating the high frequency components.

In common, deep ocean applications, the riser designer is faced with complexities such as sheared current profiles, high mode number response, marine growth, and the desire to use strakes only for a limited portion of the riser. In such cases, one must take into account the hydrodynamic damping that occurs on bare or straked regions that are not VIV power-in regions. Popular VIV response prediction programs, such as SHEAR7, VIVA, and VIVANA, can perform such calculations and typically predict substantial amounts of hydrodynamic damping on the riser. The dimensionless damping parameter, c^*, introduced by Vandiver [14] and extended to flexible cylinders by Rao and Vandiver in Ref. [15] captures the effects of damping even in cases with partial strake coverage and is much better suited at predicting response amplitudes of risers in realistic conditions. Their work shows that the VIV response amplitude, A_f^*, is inversely proportional to the dimensionless damping parameter, c_f^*, and when plotted on a logarithmic scale, the curve resembles an inverse S-curve (see dashed line in Fig. 12).

For a flexible cylinder, the dimensionless damping takes the following form:

$$c_f^* = \frac{2c_f\omega}{\rho U_f^2} \tag{4}$$

where c_f is the equivalent damping coefficient that includes the hydrodynamic and structural damping contributions, ω is the excitation frequency, ρ is the fluid density, and U_f is the equivalent flow speed. The subscript f is used to identify that this form of the dimensionless damping parameter and the quantities it involves are computed after trying to model the flexible cylinder as an equivalent rigid cylinder that dissipates the exact same amount of power as the flexible cylinder [15].

It is beyond the scope of this paper to present a full analysis of the dimensionless damping parameter c_f^*. Instead, it will only be briefly discussed here in order to explain why the response

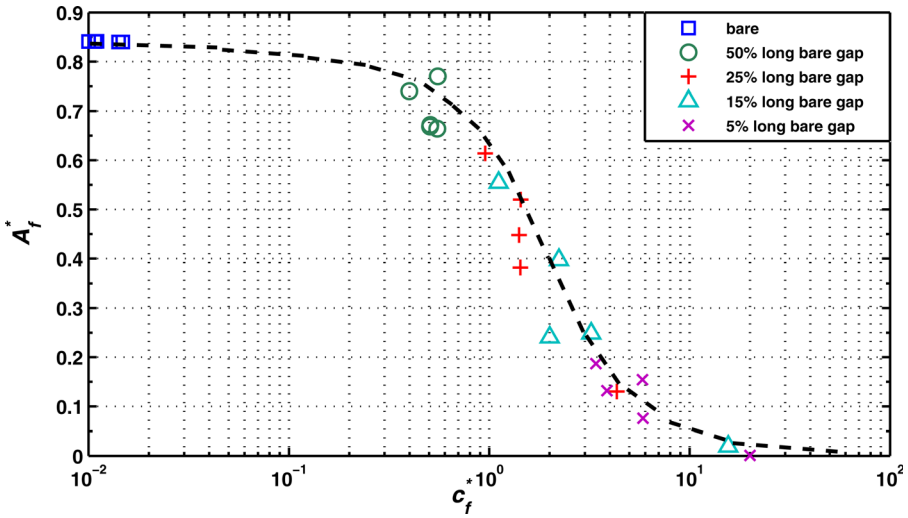

Fig. 12 Dimensionless response amplitude, A_f^*, versus dimensionless damping parameter, c_f^*, computed with SHEAR7

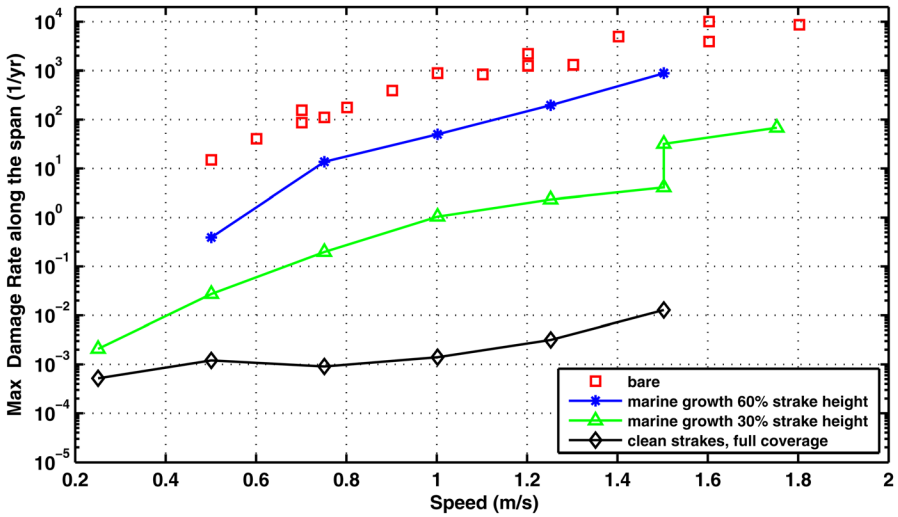

Fig. 13 Maximum damage rate (1/yr) at any location along the span versus towing speed (m/s) in uniform flows

amplitude for certain configurations of strake coverage shows a strong dependence on the flow speed whereas others do not. Close examination of Fig. 9 shows that the response amplitude for the 15% and 25% bare gap cases increases rapidly with flow speed. This increase in amplitude is much larger than what could be attributed to Reynolds number effects [5] and only seems to affect two specific strake configurations. This happens because these strake configurations (at the speeds tested) have c_f^* values that fall in the region where the VIV response amplitude depends strongly on the c_f^*.

SHEAR7 was used to model some select cases from Fig. 9 and to compute the dimensionless response amplitude A_f^* and the dimensionless damping parameter, c_f^*, the results are shown in Fig. 12. Modeling the partially strake covered cases in SHEAR7 confirms that c_f^* for the configurations with a 25% and 15% long gap happens to fall exactly in the range where A_f^* depends heavily on the value of the dimensionless damping. In contrast, the 50% long gap cases have c_f^* values that place them near the upper portion of the curve where the predicted response amplitude is not very sensitive to the value of the dimensionless damping parameter. Finally, the bare cases are predicted to have even smaller c_f^* values which reflect the small amounts of structural damping present and the absence of hydrodynamic damping since they are exposed to uniform flows and as such the entire riser length can be a power-in region. The very small c_f^* for the bare cases places them on a portion of the A_f^* versus c_f^* curve where the response amplitude is not at all sensitive to changes in c_f^* values.

4.4 Marine Growth. Figure 13 reveals the profound effect that marine growth can have on the VIV suppression effectiveness. The figure is a plot of the maximum damage rate along the span versus current speed in uniform flows for the two different amounts of simulated marine growth tested. The figure also includes the bare pipe and the clean, fully strake covered results which, as would be expected, bracket the response.

The addition of marine growth between the strake's fins essentially reduces their height making them less efficient. By the time the marine growth has covered 60% of the fin height, the cylinder cross section starts resembling a cross section of larger effective diameter with short and stubby fins. This is evident from the spectra in Fig. 14 where it is clear that the response frequency has decreased after the addition of the simulated marine growth. The plot shows the response spectrum as calculated from the average of all 30 CF strain gauges.

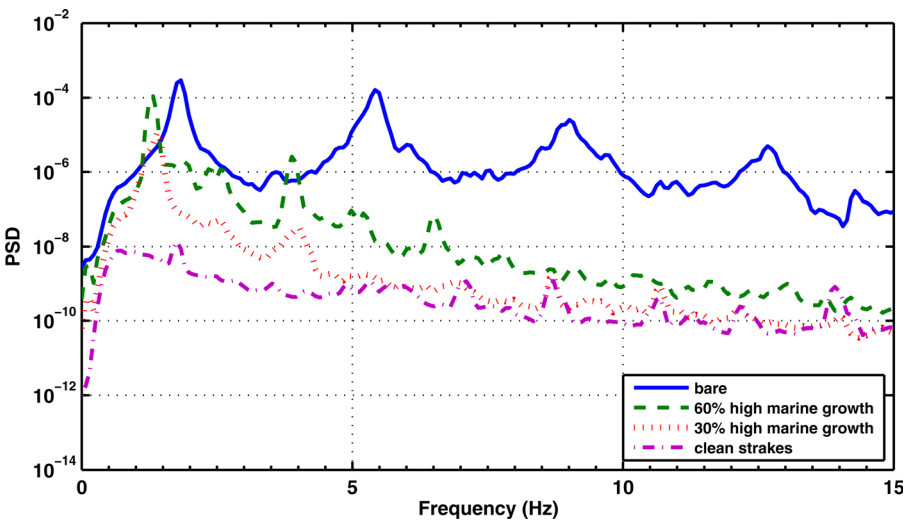

Fig. 14 Averaged PSD from all CF sensors for uniform flow of 1 m/s, effects of marine growth

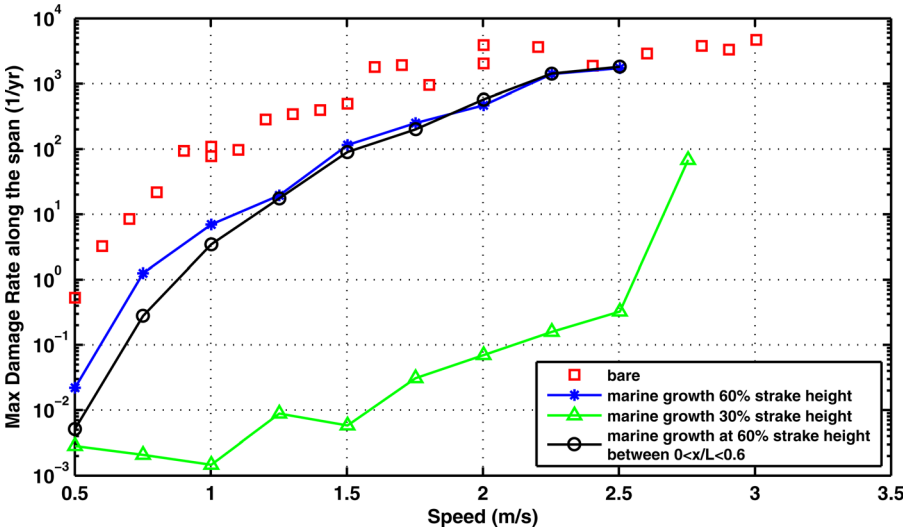

Fig. 15 Maximum damage rate (1/yr) at any location along the span versus towing speed (m/s) in sheared flows

Figure 15 shows the effect of marine growth on fully straked cylinders exposed to sheared flows. This figure also includes the very interesting case of a fully straked riser with marine growth (60% high) only applied in the region $0 < x/L < 0.6$, i.e., the high-speed end. This situation is very similar to what happens in the ocean where marine growth affects only the upper portion of a very long submerged structure.

Even though only a portion of the straked cylinder is covered in marine growth, the response is very similar to that of the cylinder fully covered in marine growth of the same height. This happens because in both situations, the high-speed end is the power-in region [12]. At certain speeds, the slightly lower response of the cylinder partially covered in marine growth could be explained by the fact that the clean strakes, which are located in the power-out region, provide more hydrodynamic damping than the marine growth covered strakes.

As mentioned earlier, the marine growth was not applied on the sides or tip of the fin but only on the portion of the strake between fins (see Fig. 2). Unfortunately, there is no experimental data available to the authors describing how the suppression capabilities of a straked flexible cylinder would change had the fin's sides and tips been covered with simulated marine growth.

5 Conclusions

The first part of this work proposes a framework for determining the magnitude and location of the most damaging combination of CF and IL bending strain around the circumference of the pipe's cross section. The results show that this usually occurs at or very close to the pure CF direction. In any case, the most damaging combination of CF and IL stress, in terms of damage rate, is usually very similar in magnitude to the pure CF damage rate and always of the same order of magnitude. This is very reassuring since most VIV prediction software only account for damage due to CF motion.

The second and main part of this work focuses on the effectiveness of different amounts of strake coverage. It is demonstrated that the concept of 'strake efficiency' is practically useless in predicting what will happen in the context of flexible cylinders perhaps with the exception of an idealized case of full strake coverage in uniform flows. The results show that even though the tests used strakes, with a suppression efficiency approaching 100%, a bare section, just 15% of the total length, is sufficient to result in noticeable VIV under uniform flow conditions. Strake efficiency, measured on a fully straked rigid cylinder, with little or no damping provides little insight when it comes to predicting the response of a riser partially covered by strakes in a sheared flow.

Additionally, the tests showed that a reduction of response amplitude of one order of magnitude will have an associated reduction in damage rate that is several times larger because of the ability of strakes to suppress the 3X and 5X higher harmonics.

Finally, the experiments demonstrated that even small amounts of marine growth, equal to 30% of the strake's fin height, are sufficient to increase the measured damage rates by an order of magnitude compared to clean strakes. Modest amounts of marine growth, equal to 60% of the fin height, are capable of negating most of the suppression benefits provided by clean strakes.

Acknowledgment

The authors acknowledge SHELL International Exploration and Production Co. for providing access to the experimental data and the SHEAR7 JIP members (BP, Chevron, ConocoPhillips, ExxonMobil, Petrobras, SBM, Shell, Statoil, and Technip) for supporting this research.

References

[1] MARINTEK, 2011, "Shell Riser VIV Tests Main Report," MARINTEK, Trondheim, Norway, Technical Report No. 580233.00.01.
[2] Lie, H., Braaten, H., Jhingran, V. G., Sequeiros, O. E., and Vandiver, J. K., 2012. "Comprehensive Riser VIV Model Tests in Uniform and Sheared Flow," ASME Paper No. OMAE2012-84055.
[3] Baarholm, R., and Skaugset, K., 2008, "Modelling and Characterization of Artificial Marine Growth," ASME Paper No. OMAE2008-57587.
[4] Skaugset, K., and Baarholm, R., 2008, "Effect of Marine Growth on an Elastically Mounted Circular Cylinder," ASME Paper No. OMAE2008-57586.
[5] Resvanis, T. L., Vandiver, J. K., Jhingran, V., and Liapis, S., 2012, "Reynolds Number Effects on the Vortex-Induced Vibration of Flexible Marine Risers," ASME Paper No. OMAE2012-83565.
[6] Rao, Z., Vandiver, J. K., Jhingran, V., and Sequeiros, O., 2012, "The Effect of Exposure Length on the Vortex Induced Vibration of Flexible Cylinders," ASME Paper No. OMAE2012-83273.
[7] Tognarelli, M. A., Slocum, S. T., Frank, W. R., and Campbell, R. B., 2004, "VIV Response of a Long Flexible Cylinder in Uniform and Linearly Sheared Currents," 2004 Offshore Technology Conference, Houston, TX, May 3–6, Paper No. OTC 16338.
[8] Crandall, S. H., and Mark, W. D., 1963, *Random Vibration in Mechanical Systems*, Academic Press, New York.
[9] WAFO-Group, 2006, "WAFO—A MATLAB Toolbox for Analysis of Random Waves and Loads—A Tutorial," Mathematical Statistics, Center for Mathematical Science, Lund University, Lund, Sweden.
[10] DNV, 2010, "Recommended Practice: Fatigue Design of Offshore Structures," Det Norske Veritas, Oslo, Norway, Recommended Practice DNV-RP-C203.

[11] Resvanis, T. L., 2014, "Vortex-Induced Vibrations of Flexible Cylinders in Time-Varying Flows," Ph.D. thesis, Department of Mechanical Engineering, MIT, Cambridge, MA.
[12] Rao, Z., Resvanis, T. L., and Vandiver, J. K., 2014, "The Identification of Power-in Region in Vortex-Induced Vibration of Flexible Cylinders," ASME Paper No. OMAE2014-24472.
[13] Resvanis, T. L., and Vandiver, J. K., 2011, "Modelling Risers With Partial Strake Coverage," ASME Paper No. OMAE2011-49817.
[14] Vandiver, J. K., 2012, "A Damping Parameter for Flow Induced Vibration," J. Fluids Struct., **35**, pp. 105–119.
[15] Rao, Z., and Vandiver, J. K., 2015, "Estimation of the Damping Parameter Governing the VIV of Long Flexible Cylinders," ASME Paper No. OMAE2015-41296.